Mechanisms of Active Control in Cylindrical Fuselage Structures

Richard J. Silcox*
NASA Langley Research Center, Hampton, Virginia
Chris R. Fuller†
Virginia Polytechnic Institute and State University, Blacksburg, Virginia
and
Harold C. Lester‡
NASA Langley Research Center, Hampton, Virginia

This paper summarizes ongoing efforts to understand and exploit active control techniques for low-frequency noise suppression in aerospace applications. Analytical models are used in an effort to understand the mechanisms of noise transmission into acoustic spaces enclosed by lightweight structures and to examine the results of experimental implementations of active control schemes. Emphasis is placed on attaining global noise reductions using a minimum number of actuators rather than localized control over many subregions. This program has demonstrated the effect of synchrophasing and interface modal filtering in limiting the modal density within the acoustic space and how strong reactive effects may occur in two-dimensional geometries. Finally, the performance of active control systems using acoustic and vibration actuators is evaluated in a simplified model. Suppressions of 10–30 dB are demonstrated, and performance is discussed in relation to the physical mechanisms and parameters of the system.

Introduction

INTEREST in the application of active noise and vibration control concepts has picked up momentum in recent years, motivated by weight-sensitive aerospace applications. Analyses indicate that systems such as the advanced turboprop aircraft, rotorcraft, and space station will all suffer from high cabin noise environments but require that a minimum of additional weight be added because of performance penalties. Active noise control is ideally suited to such applications, because of its effectiveness at low frequencies. At such frequencies, significant additional mass is traditionally required for relatively minor decreases in interior noise levels. Used in conjunction with passive techniques, this concept, with the aid of emerging computational technology, holds the promise of an improved acoustic environment with little increase in weight.

Much work in this area has dealt with the one-dimensional propagation problem, where harmonic and random noise in ducts has been significantly reduced. Many of the mechanisms and power flow relations have been derived for this simpler one-dimensional geometry, and the performance seems well understood. However, in more complex geometries, especially where interactions between different propagating media occur, the effect of active control systems on the transfer and flow of acoustic energy is only beginning to be examined.

The first work to apply active noise control in an aircraft environment was reported by Zalas and Tichy.[1] This program to reduce harmonic noise in the interior of a commuter aircraft in flight was successful over a limited spatial volume. Subsequent work by other investigators has focused on more fundamental evaluations in laboratory models or analytical studies. This work involved controlling the resonant behavior of multi-dimensional cavity modes in rigid enclosures.[2] Noise sources and control sources consisted of point monopoles or acoustic velocity sources and provided effective control only near resonance. More current research has included distributed sources arising from vibrating boundaries and the implications of resonance and off-resonance behavior[3,4] on controller performance.

Ongoing work at NASA Langley Research Center, both in-house[5–7] and under grant[8,9] has provided an improved dynamic model of a simplified fuselage by coupling the exterior acoustic source, shell response, and interior acoustic response. The analytical model and a companion experimental program have provided insight into the physical mechanisms that affect the operation of active control in coupled systems. Active control employing both acoustic and vibrational sources has been investigated. The purpose of this paper is to review these results to date. System performance is studied by demonstrating the noise suppression attained using the above-mentioned techniques and examining the mechanisms by which control is exercised over the interior noise field. Finally, it should be noted that throughout this work, emphasis has been placed on exercising control over extended spatial domains rather than attaining localized suppressions.

Analytical Model

Figure 1 shows the primary model used for the analytical development. A complete description of the analytical model is given in Ref. 10. The fuselage is represented as an infinitely long, thin, uniform, elastic cylinder of radius a and thickness h. Cylinder vibration is excited by exterior monopole sources representing propeller noise sources. The analytical solution assumes a steady-state response, and the exterior and interior acoustic fields are coupled by the radial displacement of the cylinder wall. Both the shell response and the interior acoustic response are expressed as a finite series of modes, with the interior pressure represented as

$$p(x,r,\theta) = \sum_{\beta=1}^{N_s} \sum_{n=1}^{N} S_\beta \phi_{n\beta}(x,r,r_\beta) \cos n(\theta-\theta_\beta) \qquad (1)$$

where S_β are the known external complex source strengths and

Received Oct. 31, 1988; revision received July 19, 1989.

*Aerospace Engineer, Structural Acoustics Branch. Member AIAA.
†Professor of Mechanical Engineering. Member AIAA.
‡Aerospace Engineer, Structural Acoustics Branch.

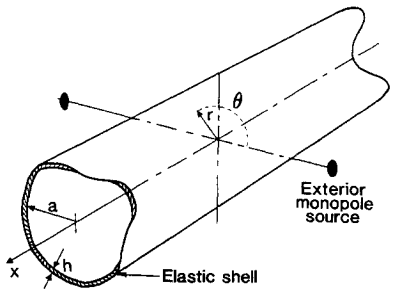

Fig. 1 Analytic model of cylindrical fuselage.

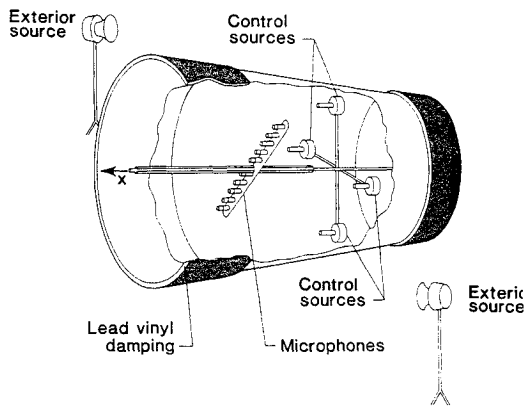

Fig. 2 Schematic of NASA test apparatus using acoustic control sources.

N_S is the number of external sources ($N_S = 2$ in this paper). The source modal distribution functions $\phi_{n\beta}$ are given in Ref. 10. These functions involve inverse Fourier transforms, with integrands defined in terms of complex Bessel functions and the various shell parameters. Note from Eq. (1) that the solution is represented as a finite sum of N azimuthal modes. Both external monopole sources were located at the same radial distance, r_β, from the axis but at azimuthal positions of $\theta_\beta = 0$ and π, as shown in Fig. 1. Equation (1) is used to predict the interior pressure and to illustrate the mechanisms inherent in the experimental results.

A similar expression for the shell displacement response W_{ns} can be derived in terms of the same azimuthal mode expansion and, from this, an expression for the modal coupling factor relating the modal response of the shell displacement to the modal pressure response of the interior cavity is obtained as Eq. (2).

$$\frac{P'_{ns}(r)}{W_{ns}} = \Omega^2 \rho_f \frac{C_L^2}{a} \frac{J_n(k_s^r r)}{k_s^r J'_n(k_s^r a)} \tag{2}$$

where $k_s^r a = \sqrt{(\Omega C_L/C_F)^2 - k_{ns}^2 a^2}$ is the radial wave number and k_{ns} the free axial wave number in the cylinder for a mode (n,s), obtained by solving the normal mode dispersion equation of the system. The term P'_{ns} is the circumferential pressure amplitude in the (n,s) mode evaluated at r. Fluid density is ρ_f, and the speed of sound in the fluid and shell is C_F and C_L, respectively. The nondimensional frequency is given by $\Omega = 2\pi fa/C_L$. Equation (2) describes the coupling between the shell and interior acoustic motion for the mode (n,s) and is the basis of the interface modal filtering effect to be demonstrated in the following sections. Only modes in which the motion is predominantly normal shell response are considered. Therefore, Eq. (2) is used to evaluate how effectively shell motion will drive the interior acoustic field for a particular mode (i.e., modal coupling coefficients).

For the results to be presented, both the shell motion and the interior acoustic response will be expanded in terms of azimuthal modes. This representation will have the form of

$$Y(\theta) = \sum_{n=1}^{N} A_n \cos n\theta + B_n \sin n\theta \tag{3}$$

where $Y(\theta)$ represents the azimuthal distribution of either the acoustic pressure or shell acceleration in terms of a Fourier series of azimuthal modes having coefficients A_n on the cosine terms and B_n on the sine terms. The sum is taken over a finite number of modes representative of the response being described. Further, the coefficients, taken generally as complex constants in this paper, are functions of axial position in the shell and axial and radial position in the interior acoustic space.

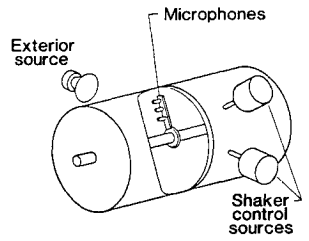

Fig. 3 Schematic of VPI&SU test setup using vibration control sources.

Experimental Apparatus

The experimental results to be presented came from two test facilities. An active control experiment using interior noise sources was performed at NASA Langley Research Center, and an experiment using vibrational control sources was performed at Virginia Polytechnic Institute and State University (VPI&SU). The two test setups were similar in their transducer arrangement and control system, using radial and azimuthal arrays of transducers to define both the interior pressure fields and shell vibration. The source control systems also operated with similar optimization algorithms.

The NASA facility is shown in schematic form in Fig. 2. The fuselage model consisted of a 1-mm-thick aluminum cylinder, 40 cm in radius and 1.2 m long. Ribs at either end supported the skin and ½-inch-thick aluminum end caps sealed the enclosure. In order to reduce interior axial acoustic reflections, the cylinder ends were covered with 15 cm of acoustic foam. Similarly, two strips of lead vinyl were attached to each end of the cylinder wall, one inside and one outside, to reduce structure-borne axial reflections in the shell.

Two exterior point sources were used on either side of the cylinder ($\theta_\beta = 0$ and π). These were driven either in-phase or out-of-phase in order to excite different primary acoustic fields within the cylinder. The acoustic field was measured by an array of 10 microphones spaced across a diameter as shown in Fig. 2. The array could be traversed in both the azimuthal and axial directions. This allowed the mapping of the interior acoustic field in all three dimensions and provided a basis for determining the performance of the active control systems. In addition, 16 accelerometers, mounted on the shell in an azimuthal array, measured the shell response at various fixed axial locations and provided an evaluation of the azimuthal modal response of the shell using Eq. (3). These were 0.3-g accelerometers and were selected to minimize the loading effects on the cylinder.

Finally, as shown in Fig. 2, four control sources were located within the cylinder all in the same axial plane as the exterior sources. These were driven in such a way as to minimize the sum of the mean squared pressures at the 10 microphone locations. Additional information on the convergence algorithm is documented in Ref. 13.

A schematic of the facility at VPI&SU is shown in Fig. 3. Here a similar experimental setup was used. The cylinder was 25.4 cm in radius, 1.245 m long, and 1.63 mm in wall thick-

ness. One exterior acoustic source provided the primary excitation of the cylinder in contrast to the two used in the NASA facility. The control was provided by either one or two mini-shakers exerting a force input at a point or points on the cylinder wall. These shakers were mounted to a stand secured to the anechoic room floor. All the excitation was in a single axial cross section.

The transducer arrangement was similar to the NASA setup, but with three microphones across a single radius rather than 10 across the diameter. Data was acquired at 24 azimuthal positions and two axial positions. Additionally, 24 accelerometers were arranged in an azimuthal array in the source plane, allowing a decomposition of the shell response into azimuthal modes.

Results

The results to be presented include an overview of the noise transmission phenomenon for the above-mentioned specialized geometries and illustrations of the performance of active control systems using either acoustic or vibration control sources. These results will be shown in terms of the azimuthal modal response, Eq. (3), of both the shell and the interior acoustic field. Contours of the interior pressure fields are presented for various exterior source conditions, and the analytical model is used to explain the measurements. The interior pressure field is shown to be a highly reactive two-dimensional sound field with large spatial variations in the acoustic response. The interface modal filtering effect is shown to influence the number of modes excited in the acoustic space, and an extension to more complicated geometries is presented. Finally, the performance of the active control systems in terms of global reductions is illustrated. The parameters influencing the performance and extent of the spatial suppressions are examined and quantified.

The cases chosen are presented in terms of a nondimensional frequency $\Omega = 2\pi fa/C_L$, where C_L is the phase speed of axially propagating waves in the shell. A value of $\Omega = 0.2$ corresponds to a 170-Hz tone in a 2-m-diam aluminum fuselage. This nondimensional frequency is representative of the second harmonic of blade passage frequency (BPF) for current commuter aircraft or approaches the fundamental BPF for the advanced turboprop aircraft.

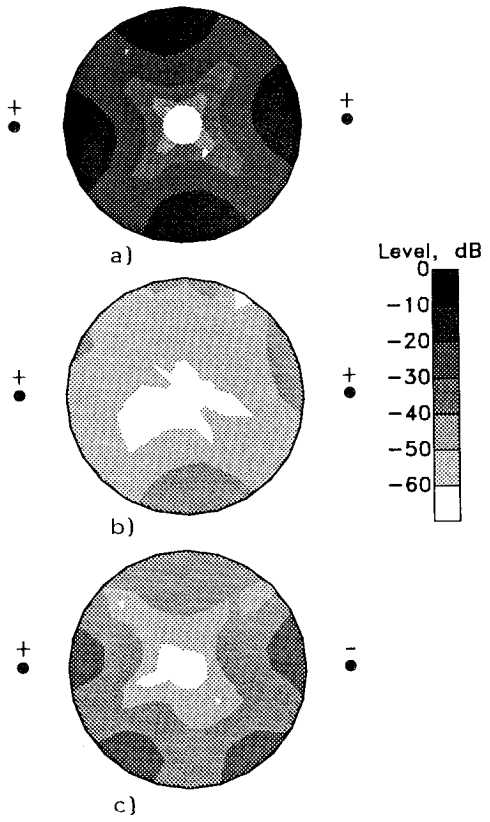

Fig. 4 Normalized pressure level contour maps for three source conditions: a) in-phase exterior sources, $\Omega = 0.22$; b) in-phase exterior sources, $\Omega = 0.10$; and c) out-of-phase exterior sources, $\Omega = 0.22$.

Noise Transmission Effects

The effect of source configuration and frequency on measured interior pressure distributions is demonstrated in Fig. 4. In the figures, the interior acoustic field is shown as a normalized pressure level contour for a specified nondimensional shell frequency ($\Omega = 2\pi fa/C_L$). The key relates the sound pressure levels (SPL) corresponding to seven gray scales in 10-dB increments. These levels are relative to the exterior SPL measured at the shell wall in the source plane at $\theta = 0$ and π. Therefore, these results indicate some measure of the transmission loss through the cylinder wall subject to the modal response of the cylindrical shell and the interior acoustic space. As will be shown, these levels are affected by the phasing of the exterior sources.

In Fig. 4a, results are presented for a nondimensional shell frequency of $\Omega = 0.22$ or 475 Hz in the NASA test facility. The exterior monopoles were operated in-phase, resulting in a dominant $n = 2$ [i.e., A_2 from Eq. (3)] azimuthal mode in the interior acoustic space. An azimuthal expansion of this pressure field shows the $n = 2$ mode 20 dB higher than the next highest mode, the $n = 4$ azimuthal mode. Correspondingly, the four-lobed pattern in the pressure field is characteristic of the $n = 2$ mode with alternate peaks in this pressure field 180 deg out-of-phase. This case is near the $n = 2$ mode resonance in the cross-sectional space, and this leads to the dominance of this mode and the rather low transmission loss, about 14 dB. At the lower frequency of 216 Hz, $\Omega = 0.10$, the measured pressure field is as shown in Fig. 4b. This is plotted to the same scale as Fig. 4a, and it is evident that the interior levels are significantly lower. Here the $n = 2$ mode is down 23 dB over that of Fig. 4a.

As an illustration of the effect of source structure on the interior pressure response, the pressure contour map is shown for out-of-phase exterior monopoles in Fig. 4c for $\Omega = 0.22$. A decomposition of the interior pressure field near the wall reveals the A_3 azimuthal mode to be approximately twice as strong as the A_2 and B_2 modes, which are of equal strengths. As discussed in Ref. 14, the out-of-phase sources should not excite the sine modes or any of the even modes [i.e. from Eq. (3), $A_n = 0$ for $n = 0,2,4,6,\ldots$ and $B_n = 0$ for all n]. However, asymmetries in the test setup and the cylinder seam accentuate the scattering effects and, thus, some B_n response and even modes are observed. It is important to note that changing the source phase by 180 deg has reduced the level of the $n = 2$ mode by nearly 30 dB over Fig. 4a and near the meaningful noise floor of the measurement. Overall, the transmission loss for this condition has increased by 20 dB for this alternate source structure.

Comparison of Figs. 4a and 4c illustrates the effect of synchrophasing or source phasing on the interior acoustic field. Dramatic reductions of interior noise are achieved using this technique because the shell modes that couple most efficiently to the interior acoustic space are reduced. Source phasing may be considered another aspect of active control as it is optimizing one source with respect to another to minimize the interior acoustic field. These results consider only the simple aspects of monopole sources; however, with the use of counter-rotating propellers, additional source phasing parameters are available and need to be integrated into the total picture of an active control system.

The coupling of the shell displacement to the interior pressure as computed by Eq. (2) is illustrated in Fig. 5. This plot relates the individual azimuthal modes in the shell to corresponding acoustic modes in the interior and does not account for the shell excitation. For a symmetric cylinder, no coupling can occur between structural and acoustic modes of different

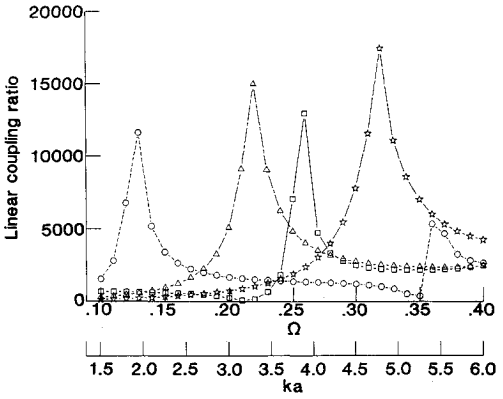

Fig. 5 Theoretical coupling ratio between the shell azimuthal modes and the cavity azimuthal/radial modes; □–, $n=0$, o---, $n=1$, Δ—·—, $n=2$, *--, $n=3$.

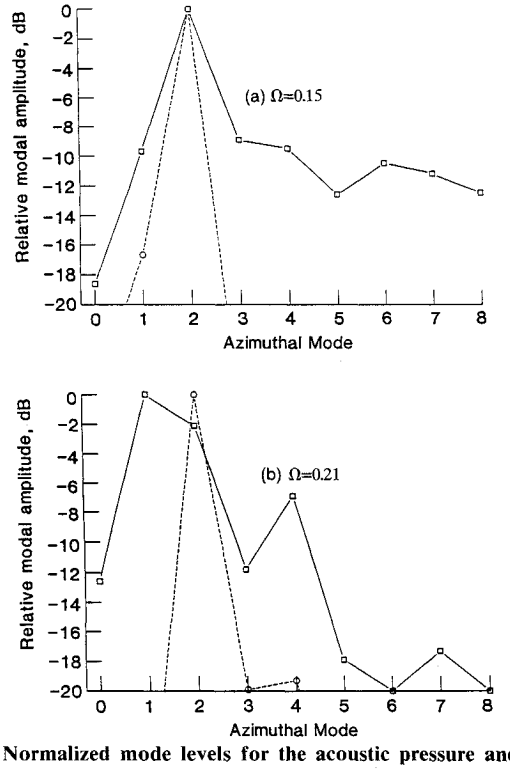

Fig. 6 Normalized mode levels for the acoustic pressure and shell displacement in the source plane; o----, acoustic modes; □–, shell modes.

azimuthal order as they are orthogonal. Therefore, for an azimuthal mode to appear in the acoustic field, it must be present in the shell. Note that the analysis is for an infinite-length cylinder and, although the test cylinders are finite, the analysis does illustrate the coupling mechanisms, trends, and magnitudes. These curves were evaluated at $r/a=0.93$, and the peaks of the curves correspond to the cut-on frequencies of the respective interior acoustic modes. Each interior acoustic radial, as well as azimuthal, mode generates a curve as noted for the $n=0$ curve, which corresponds to the first higher-order axisymmetric radial mode. However, as stated previously, only normal shell response solutions are investigated; thus, peaks in the curves correspond to coincidence between the free shell response and higher-order interior mode response. The peak for the plane wave mode or breathing mode occurs at $\Omega=0.0$ and generally is not excited.

At any given nondimensional shell frequency Ω, a distribution of shell azimuthal modes will generally give rise to one or two dominant interior acoustic modes, according to this reso-

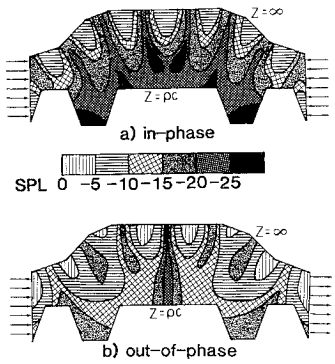

Fig. 7 Normalized pressure level contours in aircraft cabin geometry using finite-element model, $ka=3.5$.

nant behavior. This was illustrated in the cases presented in Fig. 4 where, for in-phase or symmetric excitation, a dominant $\cos 2\theta$ mode was excited both at resonance where a strong response resulted and away from resonance where a significantly reduced overall response occurred. For antisymmetric excitation (out-of-phase), a dominant $\cos 3\theta$ mode was excited but at reduced levels because the frequency was significantly below the resonance of this mode.

Figures 6a and 6b further demonstrate the filtering effect of the structural-acoustic coupling (interface modal filtering) between the shell and the acoustic cavity. Normalized modal levels for the first eight cosine azimuthal modes (A_n) are compared for the structure and the interior space. For the discussions to follow, the sine modes (B_n) were found to be of negligible amplitude in the shell, and acoustic space and references to azimuthal modes should be taken as references to cosine modes (A_n). At $\Omega=0.15$ (324 Hz), the $n=2$ azimuthal mode dominated the shell and acoustic response. However, other modes strongly present in the shell were negligible in the interior acoustic space. This is demonstrated even more dramatically in Fig. 6b, where the $n=1$ mode dominated the shell response but is not detected in the acoustic cavity response. This effect was evident throughout the tests conducted at both the NASA and VPI&SU facilities. Thus, interface modal filtering has the benefit of reducing the modes that need to be controlled in the acoustic space and has different implications for acoustic and force control inputs, as will be pointed out later.

As the responses shown so far apply only to an idealized fuselage geometry, results that model a more realistic interior geometry are taken from Abrahamson.[11,12] This analysis uses a finite-element model to approximate the acoustic response of an aircraft cross section. The reader is directed to the references for additional details of the model. Cross sections representing the free acoustic space in a two-aisle passenger cabin with overhead bins are represented in Figs. 7a and 7b. The upper boundary is a hard wall, and the lower boundary, representing seats and carpet, is given a normalized specific acoustic impedance of 1.0. The left and right boundaries are taken as piston sources (vibration sources) and driven in-phase in Fig. 7a and out-of-phase in Fig. 7b. A dominant symmetric mode response is produced in Fig. 7a, with in-phase excitation of the sidewalls. A dominant antisymmetric mode response is produced in Fig. 7b, with out-of-phase excitation. Note also the reduced levels of Figs. 7a over 7b, indicating a similar interface modal filtering effect due to the source phasing effects as previously demonstrated. This occurs even with the more localized excitation and irregular geometric and acoustic characteristics. These results, in combination with the known effectiveness of synchrophasing in aircraft, imply that the same coupling effects and cavity responses will apply for more complex geometries and that the results from the cylindrical geometry will apply to more realistic models.

Returning to the cylinder model, Fig. 8 shows a normalized plot of the predicted interior intensity and pressure fields at the

wall, $r/a = 1.0$, resulting from in-phase exterior monopole sources at $\Omega = 0.22$. The reactive behavior of the interior cross-sectional space is evident, even in this infinite duct model, from the intensity levels that are 6–20 dB down from the interior sound pressure levels. For free-field radiation from a point source, the relative levels of the SPL and intensity level would be the same. Alternate peaks of the intensity correspond to ingoing and outgoing flows of acoustic energy. Preliminary experiments confirm this effect, but more detailed measurements are needed. Here the coupling of the azimuthal modes in the intensity is apparent with the strong variation of the intensity vs θ, resulting from the interaction of the $n = 2$ mode and the $n = 4$ mode at the shell wall. This strong variation in acoustic intensity with wall position is a common characteristic of the acoustic fields measured in propeller-driven aircraft[1,14] and explains why intensity measurements in aircraft are so difficult. In effect, the wall vibration is a high-order multipole source inputting and extracting energy around the wall circumference.

Other calculations demonstrate that, by shifting the frequency slightly to the opposite side of the resonance peaks of Fig. 5, the sign of the intensity flux at the interior shell wall is changed.[15] This occurs because the resonance of the pressure response is crossed while the shell velocity response remains at the same phase. This has implications for the use of passive treatments in aircraft as the regions of energy inflow and outflow can change dramatically with slight shifts in frequency and source phasing[16] (i.e., synchrophase angle).

Active Control with Acoustic Sources

This section will illustrate the use of active noise control in the NASA cylindrical fuselage model. As mentioned in the experimental setup section, the test setup was limited to a distribution of four acoustic sources. Optimization was carried out by minimizing the sum of the squared pressures for the 10 interior microphones with the array at a fixed position. Because of the nature of the excitation forcing the interior field over a large spatial extent in one dominant mode, multimodal control was not attempted on account of the increased number of control sources necessary. To exercise control over the $n = 3$ azimuthal mode at a single cross section, an array of six control sources would be needed in order to avoid modal spillover effects.[6] This was beyond the scope of this preliminary experimental work, and the results presented are restricted to the $n = 2$ azimuthal mode.

The results presented in Figs. 9a and 9b illustrate the measured performance of the active noise control system for $\Omega = 0.22$. Figure 9a shows the pressure level map of the interior field in the source plane due only to the exterior in-phase monopoles. Here, all interior SPLs are referenced to the peak interior sound pressure for the primary source alone at $x/a = 0$. As before, this field is dominated by the $n = 2$ azimuthal mode. The operation of the active control system with four acoustic monopole sources near the wall at the horizontal and vertical radii ($\theta = 0, \pi/2, \pi, 3\pi/2$) results in the composite field (primary + control), shown in Fig. 9b. Here, the peak levels are down by more than 10 dB, and the dominant $n = 2$ mode has been reduced by over 30 dB.

The global nature of this noise reduction is illustrated by the pressure field comparisons of Figs. 10a and 10b. These figures show the primary and composite fields at the axial plane $x/a = 0.75$. The primary field of Fig. 10a is about 5 dB lower than at the source plane and is still dominated by the $n = 2$ azimuthal mode. The operation of the controller yields the composite field shown in Fig. 10b. Although the reduction in levels is somewhat less than in the source plane, the axial distribution of sound in the composite field is relatively uniform. Note here that the azimuthal $n = 2$ mode appears to be relatively strong in the composite field at $x/a = 0.75$ compared to the composite field at the source plane.

The performance of the control system for the azimuthal mode $n = 2$ is presented in Figs. 11a and 11b. Here the axial distribution of the modal amplitude and phase are plotted vs axial position for the three source conditions. The level of the primary acoustic field decays about 5 dB over an axial distance of $0.75a$. The axial distribution of the amplitude closely matches that of the control sources. The phase variation is

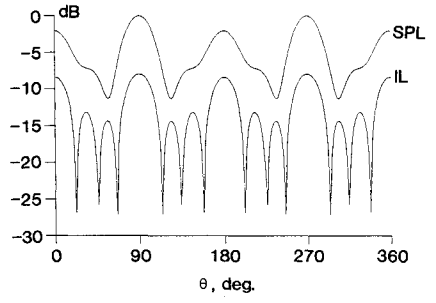

Fig. 8 Comparison of normalized SPL and intensity level predictions at the interior wall ($r/a = 1.0$); $x/a = 0.0$ and $\Omega = 0.22$.

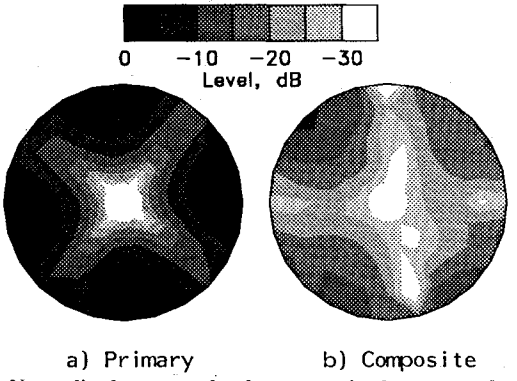

Fig. 9 Normalized pressure level contours in the source plane ($x/a = 0.0$) for primary alone and composite noise sources with in-plane exterior sources, $\Omega = 0.22$.

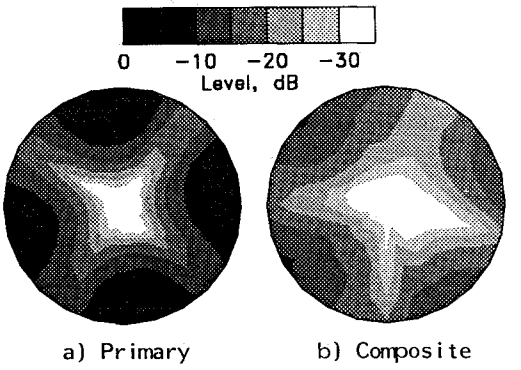

Fig. 10 Normalized pressure level contours at $x/a = 0.75$ for primary alone and composite noise sources with in-phase exterior sources, $\Omega = 0.22$.

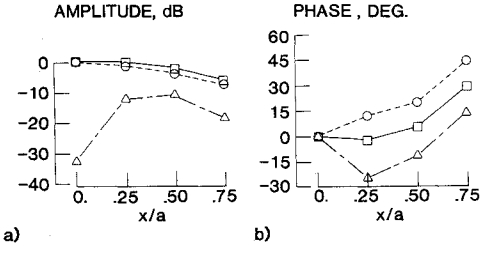

Fig. 11 Normalized mode level and phase change from source plane for $n = 2$ mode, in-phase exterior sources at $\Omega = 0.22$; □——, primary; o ---, control; Δ – – –, composite.

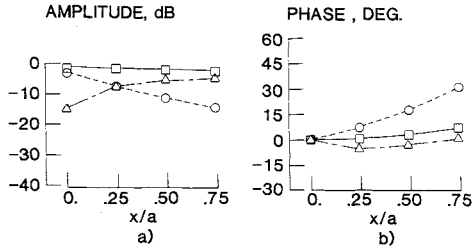

Fig. 12 Normalized mode level and phase change from source plane for $n=2$ mode, in-phase exterior sources at $\Omega=0.15$; □ – –, primary; o ---, control; Δ – – –, composite.

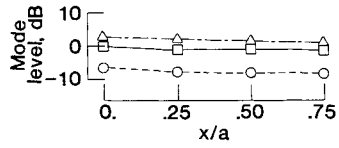

Fig. 13 Normalized shell displacement level for $n=2$ mode at $\Omega=0.22$ for three source conditions; □ – –, primary; o ---, control; and Δ – – –, composite.

negligible over a length of $0.25a$ from the source plane but then closely matches that of the control sources. At this frequency, the $n=2$ mode is just cut on and, hence, its axial wave length is very long, which is typical of the structural wave length. It is this close matching of these two $n=2$ modal wave fields that accounts for the global reduction within the enclosed cylindrical space. As noted in the pressure maps and illustrated by the composite curve in Fig. 11, the $n=2$ mode is strongly controlled in the source plane but is regenerated away from the source plane by the wall vibration. However, a consistent 10–15 dB of suppression was attained over the cylinder's interior.

At lower frequencies, away from mode cut-on, the level of suppression provided by this control system did not provide noise reductions as large as exhibited for $\Omega=0.22$; however the interior levels due to the primary sources were significantly less as demonstrated previously in Figs. 4a and 4b. The modal representation of the interior pressure field for the $\Omega=0.15$ case is shown in Fig. 12, where 15 dB of suppression for the second-order azimuthal model was obtained in the source plane. However, away from the source plane, only minimal attenuation was attained as the wave fields from the primary source and control sources did not match in their axial distributions. The axial decay of the $n=2$ mode due to the control sources was much higher than that due to the primary sources. The phase response of the primary field was characterized by the long wave lengths of the shell wave field, indicating a dominant forced response. Axial arrays of control sources may possibly be used to better match the axial characteristics of the control field to the primary field and improve the global suppression.

Finally, in order to examine the shell response for these cases, the displacement of the shell, as measured by the accelerometer arrays, is presented in Fig. 13. The response for the $n=2$ azimuthal mode is shown for the $\Omega=0.22$ case with in-phase exterior sources. The primary response was typical of all the cases, that is, a uniform axial response due to the exterior sources. Although the monopole sources are localized in these cases, the shell response seems to be excited in the source plane and propagates away with little damping. The built-up structure of aircraft would be expected to increase this damping significantly. This effect would help to reduce the spatial extent over which the active control system would have to exercise control.

Interestingly, for this case, the operation of the active control sources increases the displacement response of the shell.

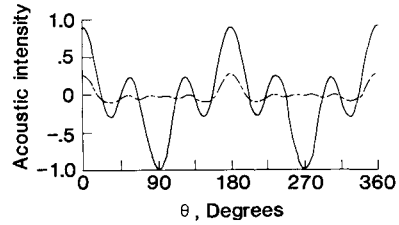

Fig. 14 Normalized radial acoustic intensity at shell wall, $x/a=0.0$, $\Omega=0.22$. ——, primary; and – – –, composite.

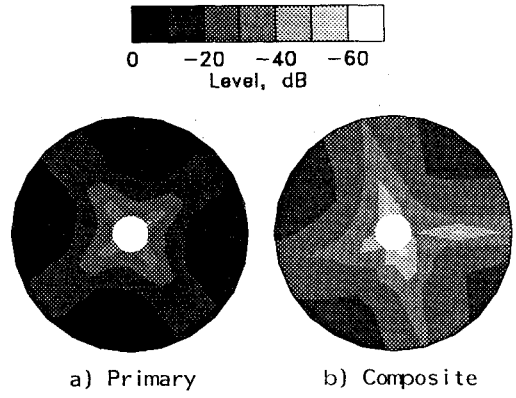

Fig. 15 Normalized pressure level contours for two source conditions using single shaker control of interior pressure field, $\Omega=0.2$, $x/a=0.0$.

This occurs because the active control system reduces the back pressure loading on the wall and, thus, the wall is essentially uncoupled from the cavity space. Because this case is at resonance for the $n=2$ mode, this back loading is larger than at other frequencies (i.e., the pressure response is larger for a given wall displacement), and the operation of the control system yields this noticeable effect. However, for none of the other frequencies tested was the composite wall acceleration discernible from the primary case alone.

Further evidence of the noise suppression mechanism is shown in Fig. 14, taken from Ref. 5. Here, the predicted interior radial intensity at the wall is shown for the primary and composite sources. A negative intensity is taken as energy into the cylinder. The primary source case shows the regions of inflow and outflow due to the dominant $n=2$ and residual $n=4$ modes. As expected, a net influx of energy occurs as a result of the slightly higher negative peak value. The composite source case demonstrates the reduced radial intensity that accompanies the operation of the control sources. Rather than absorbing the incoming acoustic energy, the control sources reduce the pressure in combination with the primary sources. The input impedance of the cavity is significantly reduced, and less energy can be transferred from the shell vibration (even with the vibration increase) to the cavity space. In combination, all the sources produce less acoustic energy than when operated alone.

Active Control with Vibration Sources

This section deals with the active control work using vibrational inputs done at VPI&SU under grant to NASA. The setup is shown in Fig. 3, and more detail is given in Refs. 9, 17, and 18. The cylindrical shell was excited with a nondimensional shell frequency of $\Omega=0.2$ by a single monopole at $\theta=\pi$. For this configuration, the sine modes (B_n) were excited to a greater extent and, therefore, the discussion will account for these modes. The optimization was carried out initially by minimizing the interior acoustic field at a single interior point ($r/a=0.925$, $\theta=0$) using a single shaker at $\theta=0$. Subsequently, an additional shaker for a second test case was added

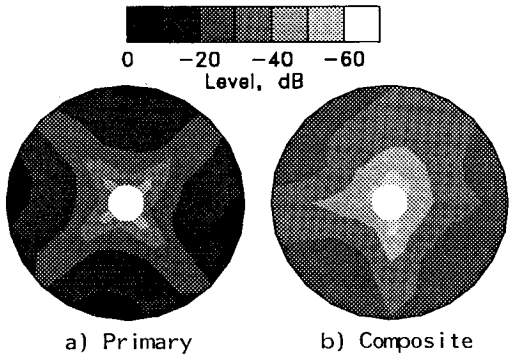

Fig. 16 Normalized pressure level contours for two source conditions using single shaker control of interior pressure field, $\Omega = 0.2$, $x/a = 1.0$.

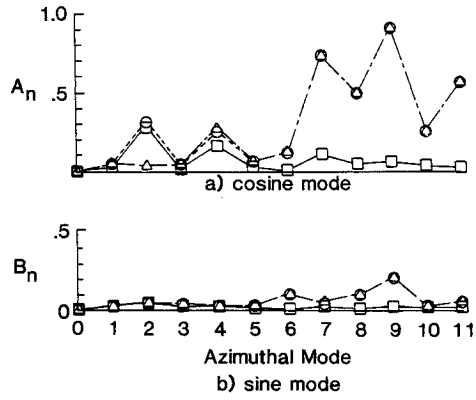

Fig. 17 Relative azimuthal mode response of shell for three source conditions, $\Omega = 0.2$; □ – –, primary; o ---, control; Δ – - –, composite.

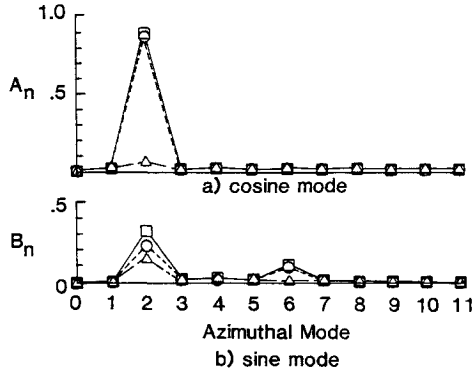

Fig. 18 Relative azimuthal mode response of interior cavity for three source conditions, $\Omega = 0.2$; □ – –, primary; o ---, control; Δ – - –, composite.

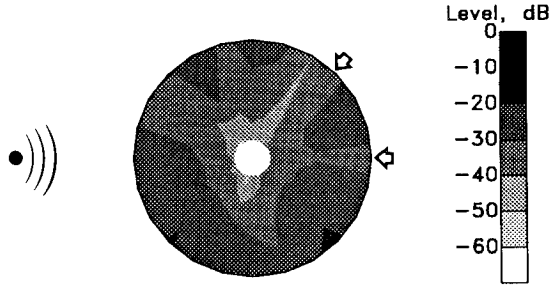

Fig. 19 Normalized pressure level contour of composite field using two control sources, $\Omega = 0.2$ at source plane.

at $\theta = \pi/4$, along with a second error microphone at $r/a = 0.925$ and $\theta = \pi/4$.

The primary acoustic field due to the single exterior source is shown as a contour of normalized SPLs in Fig. 15a. This field is characterized by a dominant A_2 azimuthal mode similar to that obtained in the NASA facility. The proximity of this frequency to resonance for this mode as noted previously (Fig. 5), is the reason for this singular dominant mode response. Operation of the active control system using a single shaker at $\theta = 0$ to control the interior sound field results in the sound field mapped in Fig. 15b. Here pressure levels have been reduced by 15 dB, and the dominant residual mode is a B_2 sine mode. Note the pressure minimum occurring at the shaker location, $\theta = 0$. Out-of-plane performance is illustrated by comparing Figs. 16a and 16b. These pressure maps show the primary and composite normalized SPL maps at $x/a = 1$, or one radius away from the source plane. The dominant $n = 2$ mode in the primary field is reduced by nearly 20 dB with the operation of the single control shaker, thus producing good global reduction.

The azimuthal mode response of the shell is shown in Fig. 17, where the dominant shell modes in the primary field are the $n = 2$, 4, and 7 cosine modes of Fig. 17a. However, the operation of the control source, while reducing the $n = 2$ modes, causes many additional higher-order modes to be excited. This is known as control spillover. As will be seen, these modes do not couple well to the interior cavity response because of the interface modal filtering described previously and are of no consequence in the acoustic field. Thus, the control spillover is constrained to the shell.

When the pressure fields are viewed in terms of the modal response plotted in Fig. 18, the significant reduction for the A_2 acoustic mode corresponds to the reduction of the A_2 shell mode of Fig. 17. The lack of any higher-order-mode contributions in the control or composite field attests to the efficiency of the filtering effect of the structural/acoustic coupling.

However, in Fig. 18, the dominant residual acoustic mode is seen to be the $\sin 2\theta$ mode B_2. Because this mode is orthogonal to the A_2 cosine mode, it is uncontrollable with this controller configuration. If a second control shaker at $\theta = \pi/4$ and an interior error microphone at $\theta = \pi/4$ are utilized, control could be exercised over this residual mode as well, The pressure field for the two control actuators operating is shown in Fig. 19 and indicates the reduction over that of Figs. 15a and 15b. Thus, the two control forces independently control the two orthogonal modes. Care must be taken in the location of the control forces and error sensors so that they efficiently couple into, and sense, respectively, the individual modes to be attenuated.

By exercising control using vibrational inputs, much of the interior control spillover effects encountered using acoustic sources can be avoided. This attacks the noise source in the shell, where the transmitting medium is essentially two dimensional, and therefore, the radiated characteristics of the control field are likely to match those of the primary field with respect to spatial distribution. Thus, a more global reduction may be attained with a reduced number of controllers. However, the price to be paid is increased control spillover into the shell response, which has implications for structural fatigue. Damping encountered in real fuselage structures will tend to reduce these spillover effects, especially for higher orders. Increasing the number of controllers will reduce this problem as well, but then acoustic sources become more attractive.

Concluding Remarks

This paper has summarized the ongoing efforts at NASA and VPI&SU to understand and exploit active control techniques. The analytical model has been shown to be a valuable asset in defining the mechanisms of the noise transmission phenomenon and guiding the application of active control schemes. This effort has centered on understanding the mechanisms that govern noise transmission into lightweight en-

closed structures and examining the results of experimental implementations of active control schemes. The emphasis in the controller design has been to attain global noise reductions using a minimum of actuators rather than localized control over many subregions.

Active control of sound fields in elastic closed cylinders by the two methods of interior acoustic sources and point forces applied at the shell wall have been independently studied. Both methods show very good global reductions, and the success of the methods has been largely demonstrated to be due to the interface modal filtering effect. Although acoustic sources appear to require more control sources to achieve global reduction than point forces, they reduce the sound field without significantly increasing shell response. Both methods have been shown to be sensitive to control actuator and sensor location. In combination with source phasing control (synchrophasing), both methods offer great potential for a variety of applications in both aerospace and nonaerospace environments.

Acknowledgments

The authors gratefully acknowledge the work of J. D. Jones and S. B. Abler for their individual contributions to the experimental work of this ongoing program.

References

[1]Zalas, J. M., and Tichy, J., "Active Attenuation of Propeller Blade Passage Noise," NASA CR-172386, July 1984.

[2]Nelson, P. A. et. al., "The Active Minimization of Harmonic Enclosed Sound Fields, Parts I, II, and III," *Journal of Sound and Vibration,* Vol. 117, No. 1, 1987, pp. 1-58.

[3]Bullmore, A. J., Nelson, P. A., and Elliott, S. J., "Active Minimization of Acoustic Potential Energy in Harmonically Excited Cylindrical Enclosed Sound Fields," AIAA Paper 86-1958, July 1986.

[4]Bernhard, R. J., and Mollo, C. G., "Prediction of Optimal Noise Controllers Using Boundary Element Methods," presented at the 111th meeting of the Acoustical Society of America, Spring 1986.

[5]Lester, H. C., and Fuller, C. R., "Mechanisms of Active Control for Noise Inside a Vibrating Cylinder," *Proceedings of NoiseCon 87,* Pennsylvania State Univ., University Park, PA, June 1987, pp. 371-376.

[6]Silcox, R. J., Lester, H. C., and Abler, S. B., "An Evaluation of Active Noise Control in a Cylindrical Shell," NASA TM-89090, Feb. 1987; Trans. ASME, *Journal of Vibration, Acoustics, Stress and Reliability in Design,* Vol. 111, July 1989.

[7]Abler, S. B., and Silcox, R. J., "Experimental Evaluation of Active Noise Control in a Thin Cylindrical Shell," *Proceedings of NoiseCon 87,* Pennsylvania State Univ., University, Park, PA, June 1987, pp. 341-346.

[8]Fuller, C. R., and Jones, J. D., "Experiments on Reduction of Propeller Induced Interior Noise by Active Control of Cylinder Vibration," *Journal of Sound and Vibration,* Vol. 112, No. 2, 1987, pp. 389-395.

[9]Jones, J. D., and Fuller, C. R., "Active Control of Sound Fields in Elastic Cylinders by Vibrational Inputs," *Proceedings of NoiseCon 87,* Pennsylvania State Univ., University Park, PA, June 1987, pp. 413-418.

[10]Lester, H. C., and Fuller, C. R., "Active Control of Propeller Induced Noise Fields Inside a Flexible Cylinder," AIAA Paper 86-1957, July 1987; *AIAA Journal,* to be published.

[11]Abrahamson, A. L., and Powell, C. A., "A Feasibility Study on the Numerical Modeling of Interior Noise Fields," AIAA Paper 86-1862, July 1986.

[12]Abrahamson, A. L., "A Finite Element Algorithm for Sound Propagation in Axisymmetric Ducts Containing Compressible Mean Flow," AIAA Paper 77-1301, Oct. 1977.

[13]Palumbo, D. L., "An Operations Manual for the Spinning Mode Synthesizer in the Langley Aircraft Noise Reduction Laboratory," NASA CR-165698, March 1981.

[14]Gade, S., "Sound Intensity Measurements Inside Aircraft," *Sound and Vibration,* Vol. 113, March 1987, pp. 32-36.

[15]Silcox, R. J., Fuller, C. R., and Lester, H. C., "Modal Coupling and Acoustic Intensity Measurements," *Journal of Sound and Vibration,* Vol. 130, No. 1, 1989, pp. 171-176.

[16]Fuller, C. R., "Analytical Investigation of Synchrophasing as a Means of Reducing Aircraft Interior Noise," NASA CR-3823, Aug. 1984.

[17]Jones, J. D., and Fuller, C. R., "Active Control of Sound Fields in Elastic Cylinders by Multi-Control Forces," *AIAA Journal,* Vol. 27, July 1989, pp. 845-852.

[18]Fuller, C. R., "Apparatus and Method for Global Noise Reduction," U.S. Patent No. 4,715,559, Dec. 1987.